Internal Medicine
The Japanese Society of Internal Medicine
doi: 10.2169/internalmedicine.0630-17
Intern Med 57: 3123-3128, 2018
http://internmed.jp

【 CASE REPORT 】

Imaging Somatostatin Receptor Activity in Neuroendocrine-differentiated Prostate Cancer

Hiroshi Mori[1], Kenichi Nakajima[1], Suguru Kadomoto[2], Atsushi Mizokami[2], Hiroko Ikeda[3], Hiroshi Wakabayashi[1] and Seigo Kinuya[1]

Abstract:
Neuroendocrine-differentiated prostate cancer (NEPC) is a rare pathophysiology. We herein report a patient diagnosed with conventional prostate adenocarcinoma before hormone therapy, which was later diagnosed as NEPC. The nadir of prostate-specific antigen (PSA) was achieved once. However, adenocarcinoma changed to NEPC in recurrence, and the serum progastrin-releasing peptide (Pro-GRP) and neuron-specific enolase (NSE) values increased. A prostate needle biopsy revealed neuroendocrine differentiation. The chemotherapy regimen was changed, and somatostatin receptor scintigraphy (SRS) helped to determine the distribution and features of lesions as well as the effects of therapy. When prostate cancer worsens despite conventional therapy, NEPC should be considered.

Key words: castration resistance, ^{111}In-pentetreotide scintigraphy, recurrence, adenocarcinoma, neuron-specific enolase, bone metastasis

(Intern Med 57: 3123-3128, 2018)
(DOI: 10.2169/internalmedicine.0630-17)

Introduction

Neuroendocrine-differentiated prostate cancer (NEPC) is a rare pathophysiological condition that arises in clinical therapy, and reports are scant. Our patient developed multiple NEPC metastases that were diagnosed using somatostatin receptor scintigraphy (SRS) after he had undergone hormone therapy.

Case Report

A man in his 60s presented with a chief complaint of pollakiuria.

History of present illness

The patient had a medical history of type-2 diabetes mellitus, hyperlipidemia, hypertension, and sleep apnea syndrome. In November 200X, the pollakiuria worsened, and his prostate-specific antigen (PSA) level increased to 772 ng/mL. Therefore, prostate cancer was suspected. His primary physician consulted a urologist at Kanazawa University Hospital, where digital rectal palpation indicated induration of the right lobe of the prostate, and a biopsy confirmed adenocarcinoma of the prostate with a Gleason score of 9 (4+5).

Contrast-enhanced CT (CE-CT) revealed cancer invasion of the bladder and seminal vesicles as well as metastasis to the pelvic and paraaortic lymph nodes but not to any other organs. The prostate cancer was staged as cT4N1M0 according to the TNM classification. Maximum androgen blockade (MAB) therapy was started, which improved the PSA level to 7.18 ng/mL compared with the pre-therapy value of 900 ng/mL. The lymph node metastases started to decease in size in July 200X, when the PSA value reached the nadir of 0.29 ng/mL. Although the patient completed the MAB therapy in October 200X, the PSA value gradually increased to within normal reference values and had reached 3.2 ng/mL by February 200X+2. Castration-resistant prostate cancer was diagnosed, and the patient was started on anti-androgen treatment. The PSA nadir (0.086 ng/mL) was achieved for a second time in June 200X. However, contrast-enhanced CT

[1]Department of Nuclear Medicine, Kanazawa University, Japan, [2]Department of Urology, Kanazawa University, Japan and [3]Department of Diagnostic Pathology, Kanazawa University, Japan
Received: December 4, 2017; Accepted: April 3, 2018; Advance Publication by J-STAGE: June 6, 2018
Correspondence to Dr. Hiroshi Mori, hirmri@gmail.com

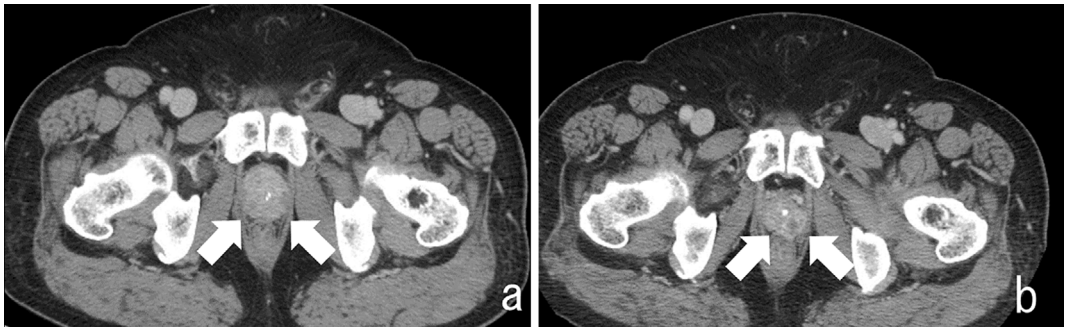

Figure 1. Imaging findings at the initial presentation and after therapy with MAB. Contrast-enhanced X-ray and CT initially showed prostate swelling (arrow), tumor invasion of the bladder and left seminal vesicle, and intrapelvic, paraaortic, and left renal lymph node metastases (a). The PSA nadir was achieved, and the prostate remained small after MAB therapy, but heterogeneous and ringed enhancement lesions were evident at the left lobe apex (b) (arrow). MAB: maximum androgen blockade, PSA: prostate-specific antigen

in November of the same year revealed a new enhanced nodule in the left lobe of the prostate. In February 200X, CE-CT revealed multiple metastases of the lungs and liver, and bone scintigraphy revealed multiple bone metastases.

Patient profile

The patient's height and body weight were 157.5 cm and 91.7 kg, respectively (body mass index 36.9 kg/m^2). His blood pressure was 157/66 mmHg, and his heart rate was 93 bpm.

Laboratory data

The blood cell counts were within the normal ranges, as follows: white blood cell 6,790/μL (neutrophils 57.5%, lymphocytes 31.4%, eosinophils 4.7%, and basophils 0.7%), red blood cell 506×10^4/μL, hemoglobin 15.0 g/dL, and platelet count 230×10^3/μL. Total protein was 6.9 g/dL (albumin 4.4 g/dL). Total bilirubin was 0.8 mg/dL, and the levels of other enzymes were as follows: aspartate transaminase 20 IU/L, alanine transaminase 35 IU/L, lactate dehydrogenase 211 IU/L, and choline esterase 427 IU/L. Other laboratory data were as follows: high C-reactive protein (1.9 mg/dL), high blood sugar (194 mg/dL), high total cholesterol (270 mg/dL), and high triglycerides (168 mg/dL). Creatinine (0.62 mg/dL) and electrolytes were normal (Na 141 mEq/L, K, 4.5 mEq/L, Cl 105 mEq/L, Ca 9.9 mEq/L). The prothrombin time was 12.1 second, and the activated partial thromboplastin time 22.2 second.

His hormone levels were within the normal ranges, as follows: free thyroxine 1.38 ng/dL, thyroid-stimulating hormone 1.14 μU/mL, growth hormone 0.14 ng/mL, cortisol 17.9 μg/dL, adrenocorticotropic hormone 22.9 pg/mL, aldosterone 106.0 pg/mL, adrenaline 0.02 ng/mL, noradrenaline 0.31 ng/mL, dopamine <0.02 ng/mL, testosterone 2.21 ng/mL, and insulin-like growth factor-1 0.1 standard deviation score.

The levels of the tumor marker PSA were markedly increased (900.19 ng/mL), while the pyridinoline cross-linked carboxyterminal telopeptide of type I collagen value was normal (3.8 ng/mL).

Imaging findings

The prostate gland was enlarged at the time of the first examination (Fig. 1a) in November 200X, and CE-CT showed heterogeneous contrast enhancement. The prostate lesion had invaded the bladder and left seminal vesicle, and metastases were found in the intra-pelvic, paraaortic and left renal lymph nodes. Neither CE-CT nor bone scintigraphy revealed distant metastasis.

At the second PSA nadir after MAB therapy in November 200X+2 (Fig. 1b), the size of the prostate had not changed, but irregular and ring-shape enhancement was identified at the apex of the left lobe of the prostate.

Chest, abdominal, and pelvic CE-CT in February 200X+3 (Fig. 2) revealed progression of the left apical lesion, new invasion to the left external anal sphincter and anal canal, and multiple metastatic lesions in the liver and lungs. Bone scintigraphy in February 200X+3 (Fig. 3a and c) showed an abnormal uptake in the vertebrae, pelvis, ribs, and bilateral humeri and femurs, indicating extensive bone metastases. SRS in March 200X+3 (Fig. 3b and d) demonstrated accumulation in several areas of the liver, findings that were in agreement with those of CE-CT and bone scintigraphy. However, plain CT did not reveal any osteolytic or osteogenic changes.

Progress of multiple metastases

The PSA value was still low at 0.37 ng/mL in February 200X+3 when multiple metastases of the lungs, liver, and bones appeared. However, the neuron-specific enolase (NSE) levels (354.2 ng/mL and progastrin-releasing peptide (Pro GRP) (119.0 pg/mL) were obviously elevated, suggesting NEPC. Therefore, etoposide/cisplatin (EP) therapy was started (Fig. 4).

A high liver uptake and bone metastases were found by SRS in March 200X+3. While the bone scintigraphic find-

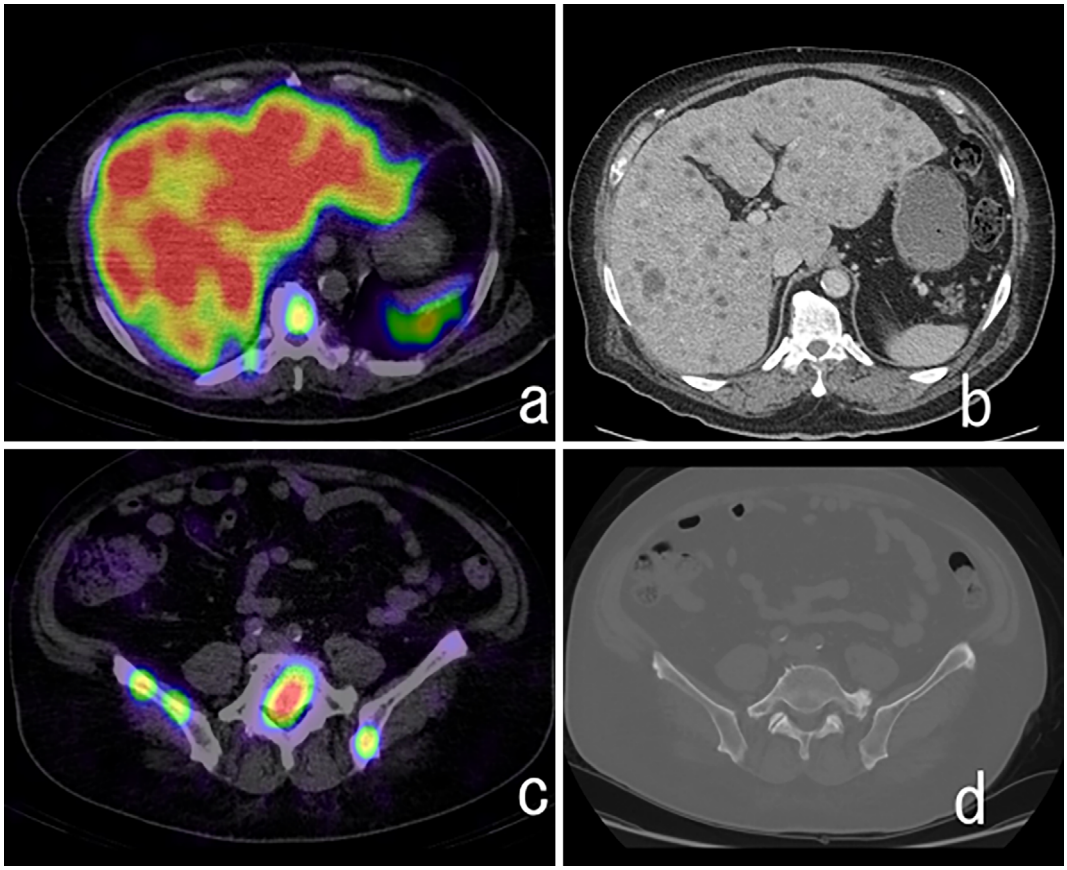

Figure 2. Findings of contrast-enhanced CT with SRS and single photon emission computed tomography (SPECT)/CT fusion imaging. Contrast-enhanced CT showed a diffuse abnormal uptake in the liver (a), which matched the multiple liver metastases on (b). Bone metastases were revealed by SRS but not by bone scintigraphy (c, d). SRS: somatostatin receptor scintigraphy

ings did not change markedly after EP therapy, SRS demonstrated a decrease in activity, indicating that the chemotherapy had been effective.

EP therapy was continued until November 200X+3. However, the patient failed to achieve remission and was transferred elsewhere to receive the best supportive palliative care.

Histopathology

The initial biopsy showed adnocarcinoma of the prostate gland (Fig. 5a). When a prostate biopy was repeated after the first EP round of therapy, the histopathological findings were poorly differentiated adenocarcinoma and neuroendocrine components (Fig. 5b). Additional immunohistochemical staining was positive for chromogranin A, CD56, and synaptophysin (Fig. 5c-e) and negative for PSA (Fig. 5f and g), and the Ki-67 index changed from 4% to 80% (Fig. 5h and i). These results were consistent with the diagnosis of neuroendocrine tumor.

Discussion

NEPC is uncommon, accounting for 0.5-2.0% of all prostate cancers. However, focal NEPC occurs in 10-100% of cases of localized prostate adenocarcinomas, and the incidence increases as the disease progresses (1-3). Massive, whole-prostate swelling and difficulty urinating are features of typical clinical episodes. The serum levels of progastrin-releasing peptide (Pro-GRP) and neuron-specific enolase (NSE) should be measured (4, 5), and NSE, chromogranin A, synaptophysin, and CD56 should also be histologically assessed (3, 5) to confirm a diagnosis of NEPC.

Imaging using 18-fluorodeoxyglucose positron emission tomography (^{18}F-FDG-PET) can help detect NEPC lesions (6). Prostate adenocarcinoma and prostatomegaly take up similar amounts of FDG. Therefore, FDG PET/CT is not useful for diagnosing prostate adenocarcinoma. However, the FDG uptake is particularly high in NEPC, so FDG PET/CT is useful for detecting primary and metastatic lesions. In addition, NEPC secretes somatostatin and expresses somatostatin receptors. By specifically targeting lesions with somatostatin receptors, SRS imaging using ^{111}In-pentetreotide might help to identify metastatic NEPC lesions. In fact, SRS using ^{111}In-pentetreotide can detect primary and metastatic lesions more effectively than FDG-PET (6-8).

In the present case, after initially treating the prostate adenocarcinoma with MAB, both the PSA value and the lesion size decreased, but the sizes of the primary prostate and metastatic lesions as well as the concentrations of NSE and Pro-GRP increased. Since SRS revealed the distribution of

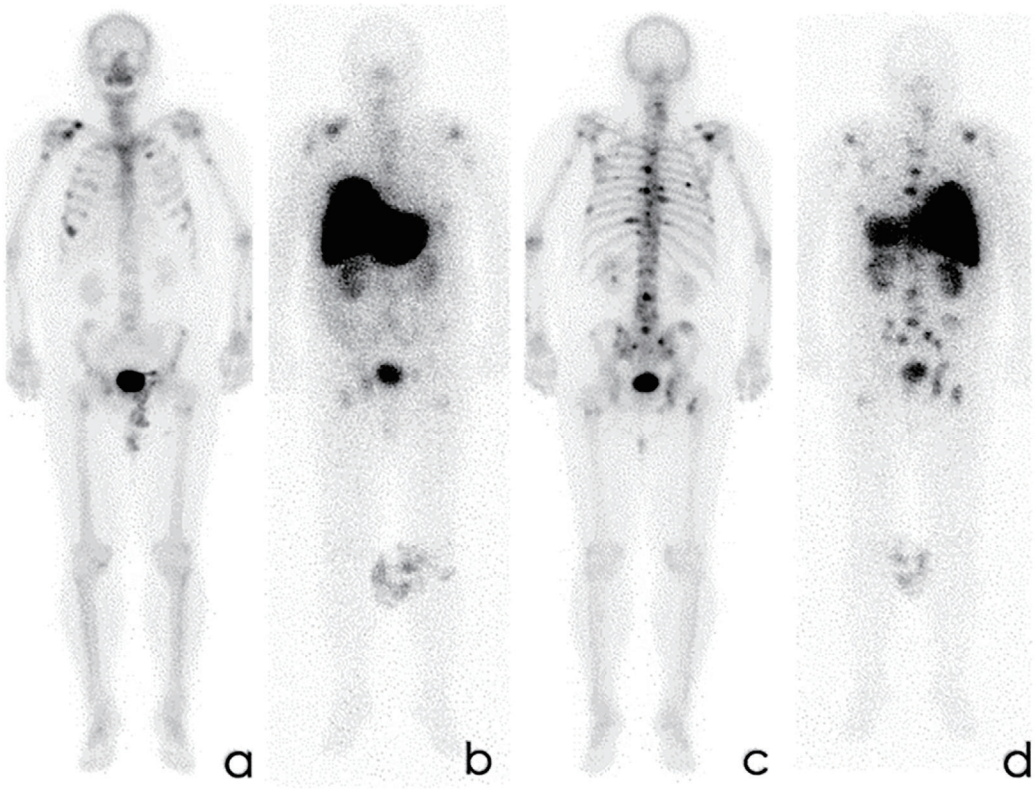

Figure 3. **Bone scintigraphy compared with SRS (a and b: anterior view, c and d: posterior view). The uptake was similarly abnormal in both scintigrams (a, c). The uptake on SRS was considered evidence of the pathological changes from adenocarcinoma to NEPC (b, d). SRS: somatostatin receptor scintigraphy**

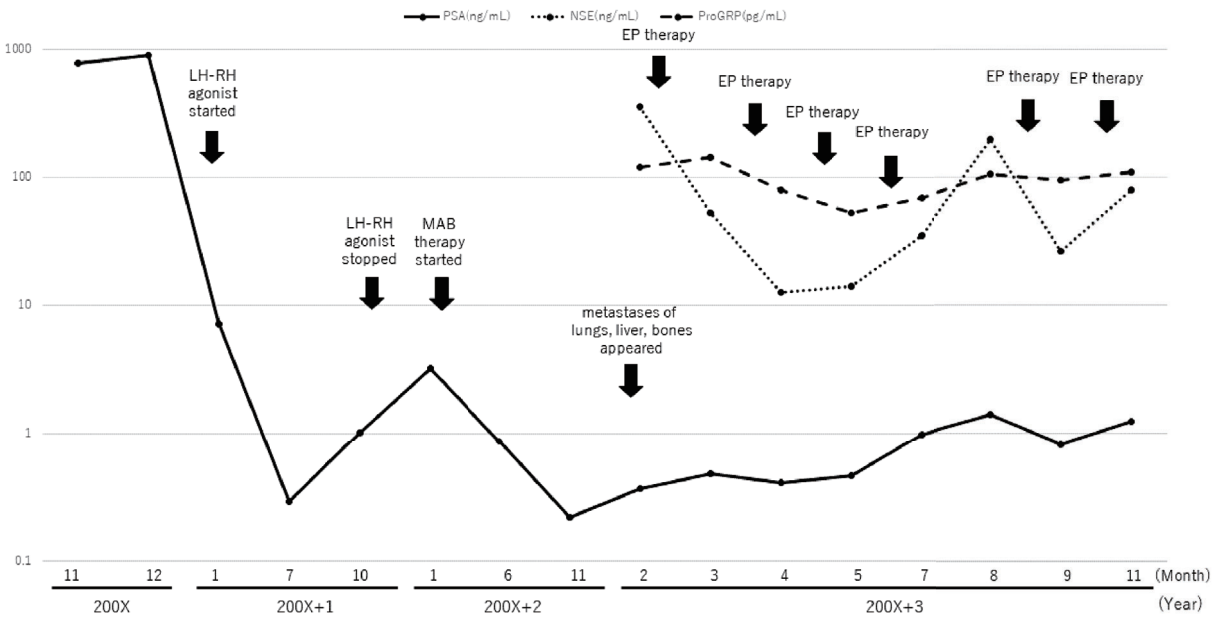

Figure 4. **The clinical course of therapy with MAB and EP. The serum PSA value decreased and archived nadir after MAB therapy. However, the primary lesion increased, and multiple metastases appeared. Differentiation into NEPC was suspected based on the increased NSE and pro-GRP values. Remission was not achieved after six courses of EP therapy. EP: etoposide/cisplatin, MAB: maximum androgen blockade, NSE: neuron-specific enolase, pro-GRP: progastrin-releasing peptide**

multiple NEPC metastases, SRS was shown to be useful for determining the final diagnosis and making therapeutic decisions. In general, while the clinical course and tumor markers help predict the differentiation of prostate cancer into

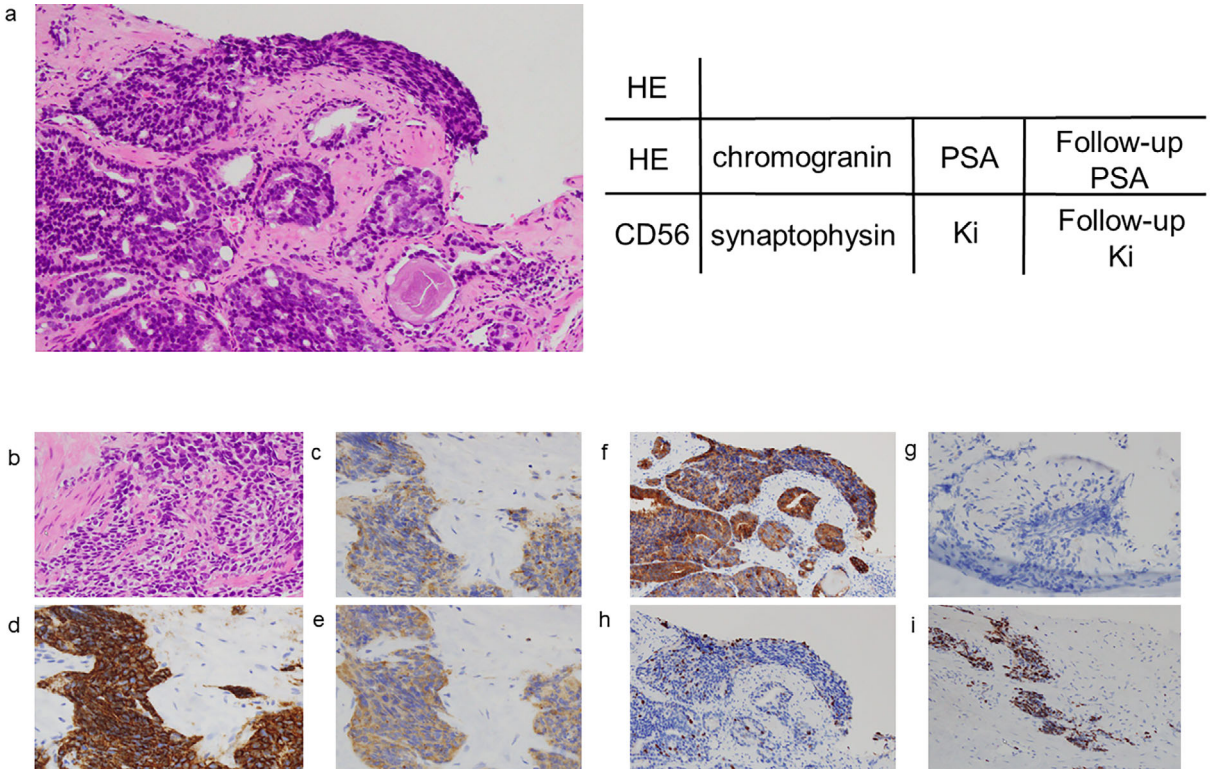

Figure 5. **Prostate needle biopsy and histopathological findings. The histopathological finding with Hematoxylin and Eosin (H&E) staining was adenocarcinoma (Gleason score 4+5=9) at 200X (a). The histopathological finding of the second biopsy with H&E staining was adenocarcinoma (Gleason score 5+5=10) with a neuroendocrine component at 200X+3 (b). The immunohistochemical findings with chromogranin A, CD56, and synaptophysin were positive at 200X+3, supporting the diagnosis of neuroendocrine tumor (c, d, e). The immunohistochemical finding with PSA was positive, and the Ki-67 index was 4% at 200X (f, h). The PSA became negative, and the Ki-67 index increased to 80% (g, i) at 200X+3.**

NEPC, the benefit of SRS imaging is in localizing lesions with neuroendocrine differentiation. Although bone scintigraphy can visualize bone metastases that are undetectable by CT, it cannot distinguish between prostate adenocarcinoma and NEPC metastases.

Another promising application of SRS imaging is its utility for visually evaluating the effects of therapy. While changes in tumor markers help predict the overall effect of therapy, changes in the uptake detected by SRS imaging can demonstrate regional improvement. Thus, SRS imaging might provide information that conventional tumor markers or imaging studies cannot disclose. Using SRS to differentiate NECP from other cancers is expected to influence treatment strategies, evaluations, and the therapeutic course significantly.

Conclusion

Diagnostic imaging of NEPC using SRS can characterize histological changes, which might be useful for the diagnosis and treatment of patients with advanced prostate cancer.

The authors state that they have no Conflict of Interest (COI).

Acknowledgement

The authors appreciate the support of Norma Foster for editorial assistance.

References

1. Abbas F, Civantos F, Benedetto PJ, et al. Small cell carcinoma of the bladder and prostate. Urol **46**: 617-630, 1995.
2. Hirano D, Okada Y, Minei S, et al. Neuroendocrine differentiation in hormone refractory prostate cancer following androgen deprivation therapy. Eur Urol **45**: 586-592, 2004.
3. Berruti A, Mosca A, Porpiglia F, et al. Chromogranin A expression in patients with hormone naive prostate cancer predicts the development of hormone refractory disease. J Urol **178**: 838-843, 2007.
4. Vamsi P, Rajen G, Kate P, Ximing JY. Neuroendocrine differentiation of prostate cancer: a review. Am J Clin Exp Urol **2**: 273-285, 2014.
5. Yashi M, Muraishi O, Tokue A. Prostatic small cell neuroendocrine carcinoma with disease progression monitored by measurement of serum progastrin-releasing peptide. BJU Int **86**: 1091-1092, 2000.
6. Daniel ES, Somali G, Lisa T, et al. Utility of FDG-PET in clinical neuroendocrine prostate cancer. Prostate **74**: 1153-1159, 2014.
7. Alberti C. Neuroendocrine differentiation in prostate carcinoma: focusing on its pathophysiologic mechanisms and pathological features. G Chir **31**: 568-574, 2010.
8. Sciarra A, Bosman C, Schillaci O, et al. Clinical evidence of neuroendocrine differentiation in a patient with prostate cancer and

bone marrow micrometastases. BJU Int **87**: 123-125, 2001.